PHYSICAL MODEL STUDY OF REFLECTION PITFALLS AND ANISOTROPY PARAMETER ESTIMATION IN A TRANSVERSELY ISOTROPIC MEDIUM

CHIH-HSIUNG CHANG[1], YOUNG-FO CHANG[2], PO-YEN TSENG[2] and CHAO-MING LIN[3]

[1] *General Education Centre, Centre of Energy Research and Sensor Technology, National Chiayi University, Chiayi 60004, Taiwan. charles@mail.ncyu.edu.tw*
[2] *Institute of Seismology, National Chung Cheng University, Chiayi 62102, Taiwan.*
[3] *Department of Electronic Engineering, Hsiuping Institute of Technology, Taichung 41280, Taiwan.*

(Received October 28, 2015; revised version accepted June 20, 2016)

ABSTRACT

Chang, C.-H., Chang, Y.-F., Tseng, P.-Y. and Lin, C.-M., 2016. Physical model study of reflection pitfalls and anisotropy parameter estimation in a transversely isotropic medium. *Journal of Seismic Exploration*, 25: 399-418.

Imaging problems due to velocity anisotropy were investigated using forward modelling. Zero-offset and constant-offset reflection experiments were performed to image spherical domes that were carved into the bottom of VTI and HTI models, respectively, along three different layout directions. Subject to velocity anisotropy, the spherical dome was projected as laterally stretched images. The curvature radius of the spherical dome was increasingly imaged in the seismic profiles due to polar velocity variation in the VTI model. An ellipsoidal dome was detected in the HTI model, instead of a spheroidal dome, due to azimuthal velocity variation. To address the problems of erroneous images in reflections, laboratory data were processed by anisotropic 2D Kirchhoff migration. Although true images were not satisfactorily restored, the effects of "lateral stretch" were significantly reduced. Due to azimuthal velocity variations, Common Depth Point (CDP) reflections acquired from different azimuths on the horizontal symmetry axis plane of the HTI model cannot be well-tied. Making use of the "mis-tie" in the CDP, which was observed in the profiles, the feasibility of estimating the Thomsen's P-wave anisotropy parameter (ε) was evaluated. Although the physical models used are relatively simple, erroneous images caused by velocity anisotropy were confirmed, and the prospect of estimating the P-wave anisotropy parameter (ε) from arrival time difference was addressed.

KEY WORDS: modelling, anisotropy, reflection, image, migration, CDP.

0963-0651/16/$5.00

INTRODUCTION

Anisotropy is ubiquitous in the earth's upper crust. In the presence of anisotropy, the velocity of a seismic wave varies with the propagation direction, a phenomenon called velocity anisotropy. Due to velocity anisotropy, spatial misposition of clear reflections becomes an inevitable problem in reflection seismology. Anisotropy not only causes positioning uncertainty of a reflection event but also increases the complexity of data processing (Vestrum and Fowler, 2005; Holt, 2006; Vestrum and Lawton, 2010). Erroneous anomalies due to omission of anisotropy effects lead to misinterpretation, especially from wide-azimuth and far-offset data (Wild, 2011). Transverse Isotropy (TI) is the simplest case of velocity anisotropy of geophysical interest. A TI material has a rotational symmetry axis and uniform physical properties in all directions on the isotropic plane, which is perpendicular to the symmetry axis. Mispositioning and defocusing effects induced by TI media have been observed by Isaac and Lawton (1999) using both field and physical model studies.

When analysing the reflections obtained from a Vertical Transverse Isotropy (VTI) model, a modified version of ridge and fault seismic models (French, 1974; Martin et al., 1992) showed that the ridge in the image was laterally stretched due to velocity anisotropy. They concluded that the curvature of the ridge can only be reliably imaged or reconstructed in the case of isotropy. In later physical model studies, Okoye et al. (1995) and Okoye and Uren (2000) demonstrated the mutuality of velocity anisotropy in the Fresnel zone dimension and spatial resolution, as well as its impact on image quality. Laboratory results reveal that the effects of velocity anisotropy on lateral resolution also relate to the orientation of the symmetry axis and the anisotropy parameter δ^* (critical near-vertical anisotropy). A review of the significance of seismic anisotropy and detailed historical analysis in exploration geophysics can be found in Thomsen (2002) and Helbig and Thomsen (2005).

In the development of exploration seismology, a forward model study is always considered as the robust tool. Making use of a scaled physical model, the complexity of wave phenomena can be accurately assessed and a sophisticated geological model is reliably described. To demonstrate that erroneous images can be obtained from a Transversely Isotropic Medium (TIM), both zero-offset and constant-offset experiments were carried out in this study to image a spherical dome from VTI and Horizontal Transverse Isotropy (HTI) models. Laboratory data show that in the presence of anisotropy the true geometry of the spherical dome cannot be accurately imaged. Furthermore, azimuthal velocity of the HTI model causes Common Depth Point (CDP) reflection on the horizontal symmetry axis (or orthogonal) plane, detected at different arrival times. Motivated by the "mis-tie" in the arrival times of reflections originating from a CDP, the feasibility of Thomsen's P-wave anisotropy parameter (ε) estimation is evaluated.

MODELLING AND LABORATORY MEASUREMENT

Phenolite is made of interlaced resin and paper. Due to its layered composition, phenolite has been widely used to study elastic wave propagation in anisotropic media, both TI and orthorhombic (Okoye et al., 1995; Waluyo et al., 1995; Grechka et al., 1999; Mah and Schmitt, 2003). The TI properties of the phenolitic block used in this study were tested in advance to facilitate our laboratory work. The five independent elastic constants of the phenolitic block, normalized by density (1.4×10^3 kg/m^3), are as follows: $A_{11} = 16.56$, $A_{13} = 4.47$, $A_{33} = 8.46$, $A_{44} = 2.16$ and $A_{66} = 4.73$ ($\times 10^6$ m^2/s^2). Using the five elastic constants, Thomsen's (1986) three anisotropic parameters (ε, γ and δ) could be readily deduced and were calculated to be 0.48, 0.60 and 0.04, respectively. Because the five independent elastic constants are premeasured, Fig. 1 shows the incident angle dependence of propagating phase and group velocities. Although the anisotropy parameters of phenolite are higher than those

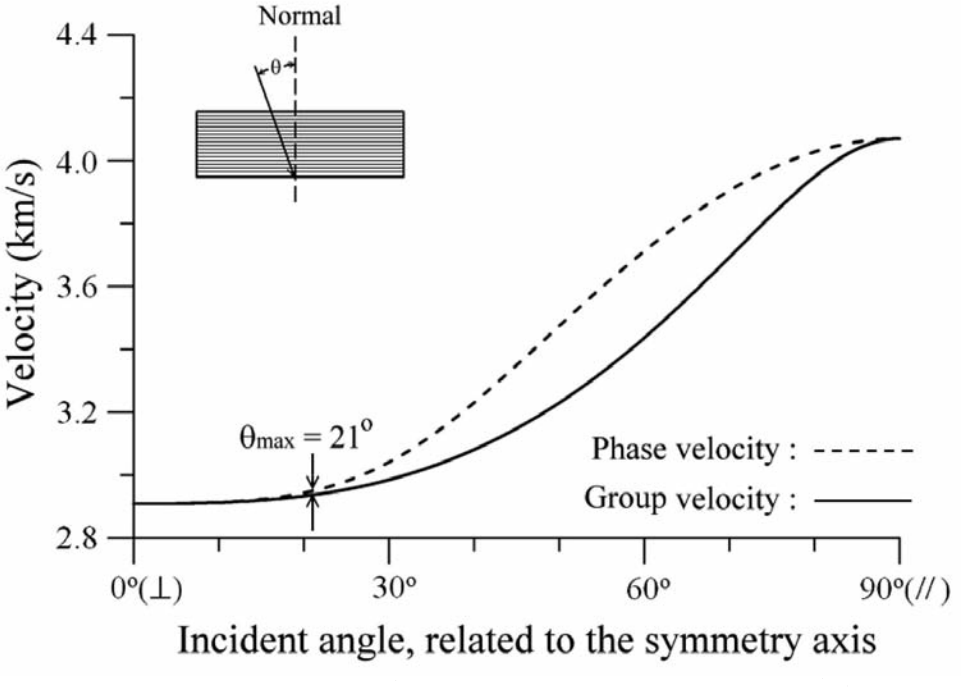

Fig. 1. Group and phase velocities vs. incident angle of the modelling Phenolite. Abscissa is used for the incident angle with respect to the symmetry axis, the phase angle for phase velocity and the ray angle for group velocity. The maximum incident angle in our laboratory operation was computed as 21 degrees.

encountered in the field, they allow magnification and easy observation of seismic wave propagation in a TIM. In the laboratory, dual TI models were individually machined from the same phenolitic block. The first model had its axis of symmetry oriented vertically (VTI), while the second had its axis of symmetry oriented horizontally (HTI). Figs. 2(a) and 2(b) show pictures of the scaled TI models. Both VTI and HTI models are the same size, with dimensions of 80 mm (L) × 80 mm (W) × 25 mm (H) [Fig. 2(c)]. A spherical dome with a diameter of 30 mm at its base and a height of 5 mm was carved into the bottom of each model.

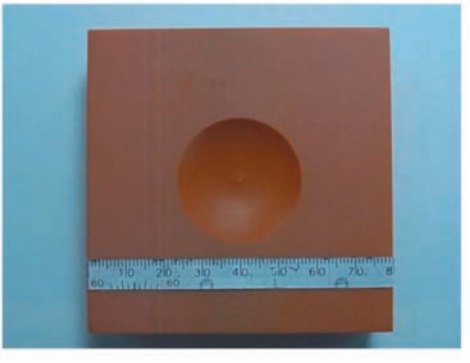

(a)

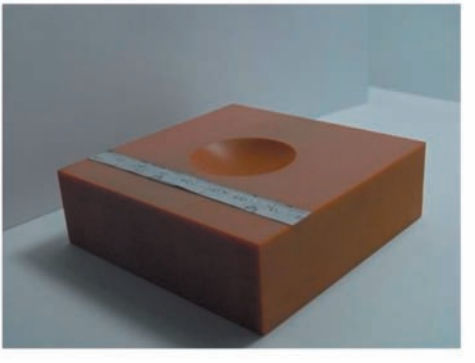

(b)

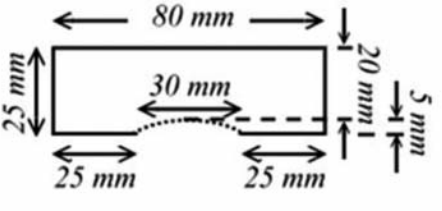

(c)

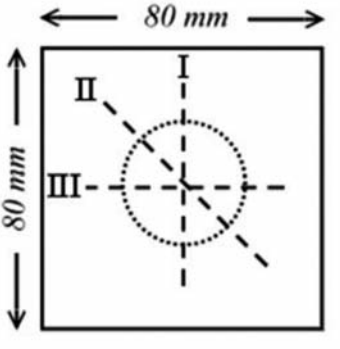

(d)

Fig. 2. Depictions of the TI model and the arrangements of survey lines: (a) view from bottom, with the symmetry axis parallel to the ruler; (b) side-view from bottom; (c) dimensions of the dome model; (d) arrangement of the survey lines (dashed).

In laboratory manipulation, two P-type transducers (PANAMETRICS V1091) with a central frequency of 5 MHz and a diameter of 3 mm were used to implement the reflection experiments. The active transducer(s) was/were driven by a PANAMETRICS 5058 pulser-receiver to record zero-offset reflections in pulse/echo mode and constant-offset reflections in double probe mode. Fig. 2(d) shows the layout of the reflection experiments. All three survey lines intersect at the projection of the apex of the spherical dome. When acquiring constant-offset reflections, the spatial interval between the active transducers was fixed at 15 mm. During data acquisition, the active transducer(s) was/were simultaneously moved 2.5 mm in the same direction for successive measurements. Each reflection observation consisted of 5000 sampling points sampled at 8 ns, i.e., 40 μs in total. Recorded signals were amplified, filtered and sent to a TEKTRONIX TDS-5032B digital oscilloscope. Finally, the observed signals were digitized and downloaded to a PC486, i.e., a computer with an Intel 486 CPU, via IEEE-488 GPIB for further processing, analysis and interpretation.

RESULTS

In this study, we evaluated the effects of velocity anisotropy on seismic images. Reflections were acquired along three different directions (Fig. 2(d)]. In the case of HTI, Lines I, II and III run parallel to, diagonal to and perpendicular to the layering direction of the model, respectively. Both zero-offset [Fig. 3(a)] and constant-offset [Fig. 4(a)] reflections were recorded to reveal distorted images obtained in the presence of VTI. Similarly, zero-offset [Figs. 5(a) and 6(a)] and constant-offset [Figs. 7(a) and 8(a)] images were acquired for the HTI model. To improve the reliability of the images, the laboratory observations [Figs. 3(a)-8(a)] were processed by anisotropic 2D Kirchhoff migration. Migration outputs are shown in Figs. 3(b)-8(b). Along the abscissa, the trace with an apex at the centre of the reflection section is the projection of the dome structure apex to be imaged. The icon shown in the upper right corner indicates the orientation of the survey line (solid) with respect to the layering of the HTI model.

Reflections in the VTI model

Profiles acquired for zero-offset and constant-offset reflections look identical, although the observations were made along three different directions. One of the zero- offset reflections collected for the VTI model is shown in Fig. 3(a). The high resemblance of the images observed in the profiles due to polar velocity variations in VTI indicates that a spherical dome was imaged. However, the base of the imaged dome is laterally extended by 58%. In order to determine

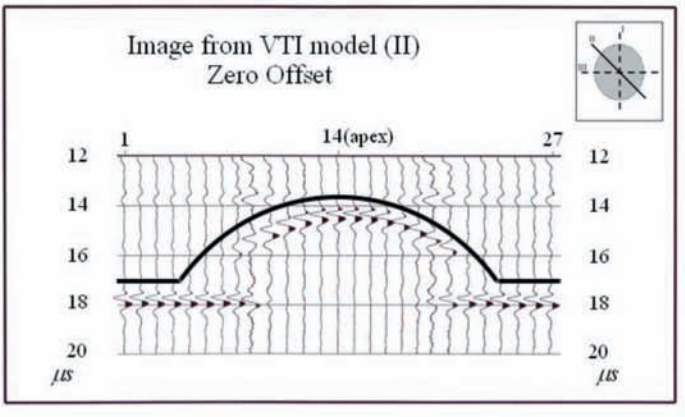

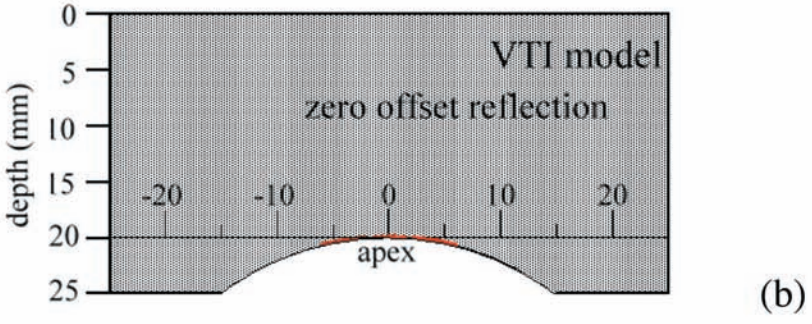

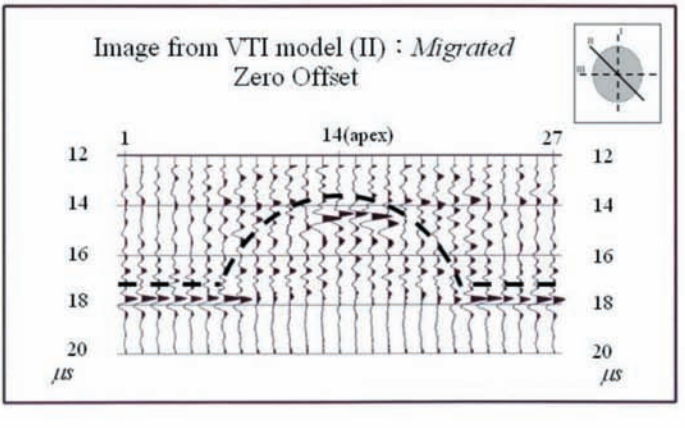

Fig. 3. Due to polar velocity anisotropy in VTI model, (a) shows one of the zero-offset reflections. In the profile, the imaged structure is delineated by the solid curve. (b) Theoretical reflection points (dots line above the apex) computed by Fermat's principle. (c) Output of the anisotropic 2D Kirchhoff migration. Reflected raypaths deviate from the normal, hence, insufficient reflections were acquired from the curvature side of the dome structure.

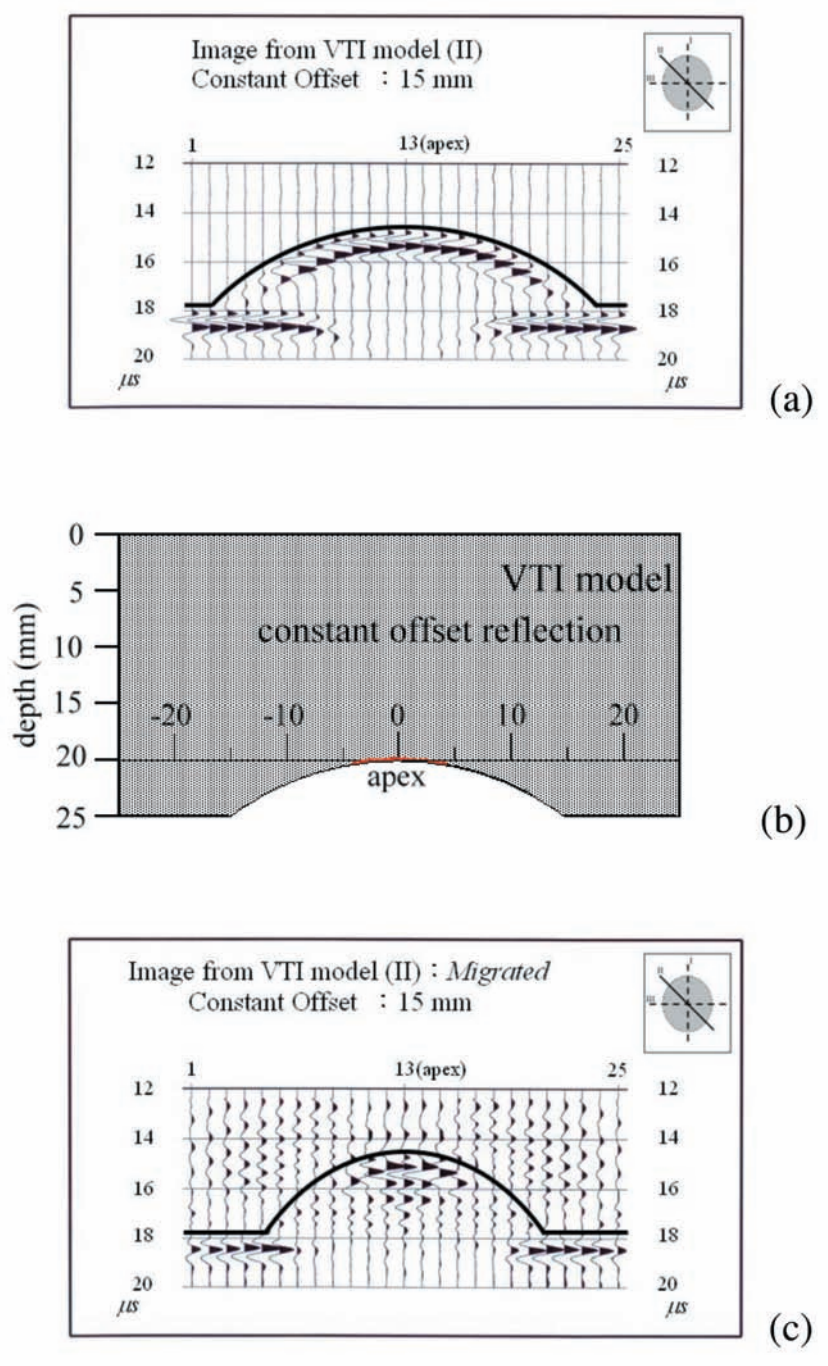

Fig. 4. (a) One of the constant-offset reflections collected for the VTI model. The imaged spherical dome possesses a larger radius compared to the created spherical dome. (b) Theoretical reflection points (dots line above the apex) computed by Fermat's principle. (c) Output of the anisotropic 2D Kirchhoff migration.

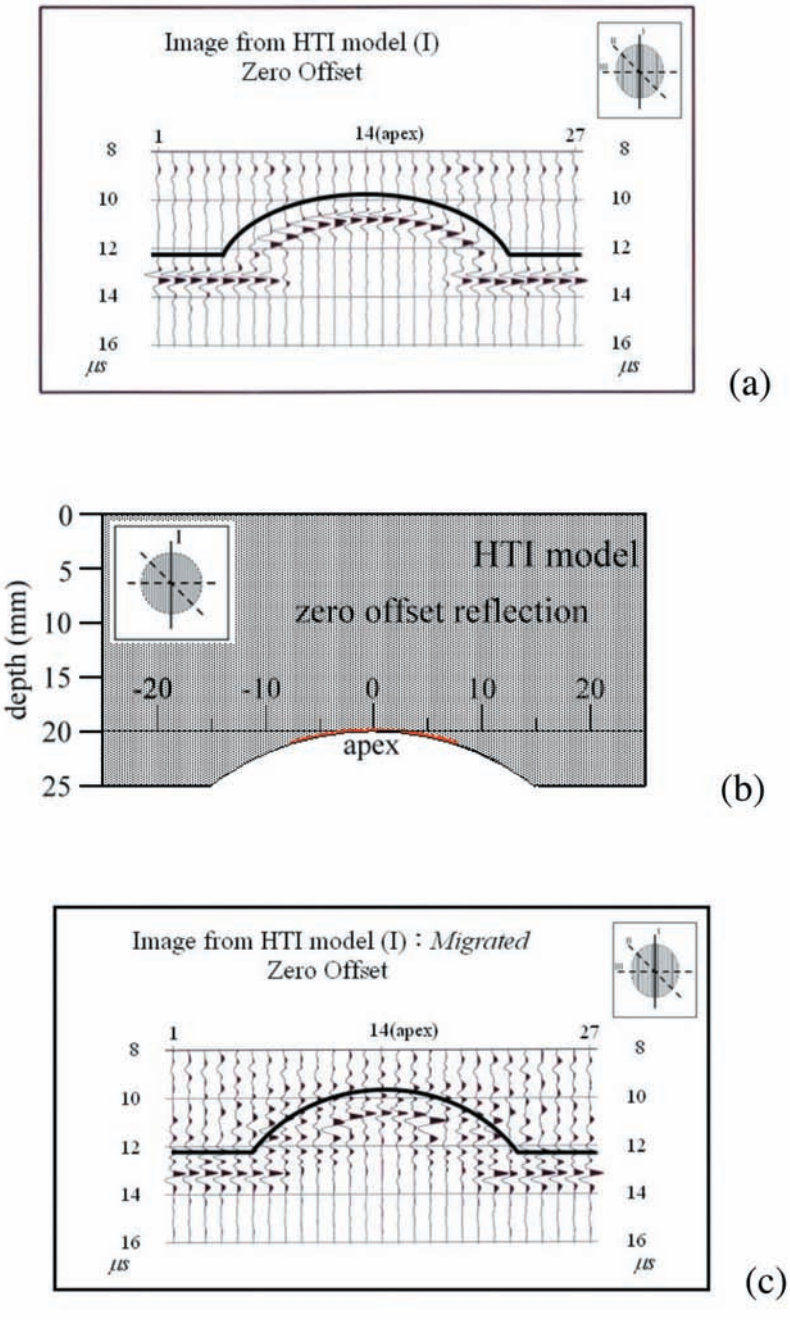

Fig. 5. (a) Zero-offset reflections acquired from the HTI model in the layering direction (I). The icon shown in the upper right corner indicates the orientation of the survey line (solid) with respect to the layering of the HTI model. (b) Theoretical reflection points (dots line above the apex) computed by Fermat's principle. (c) Output of the anisotropic 2D Kirchhoff migration.

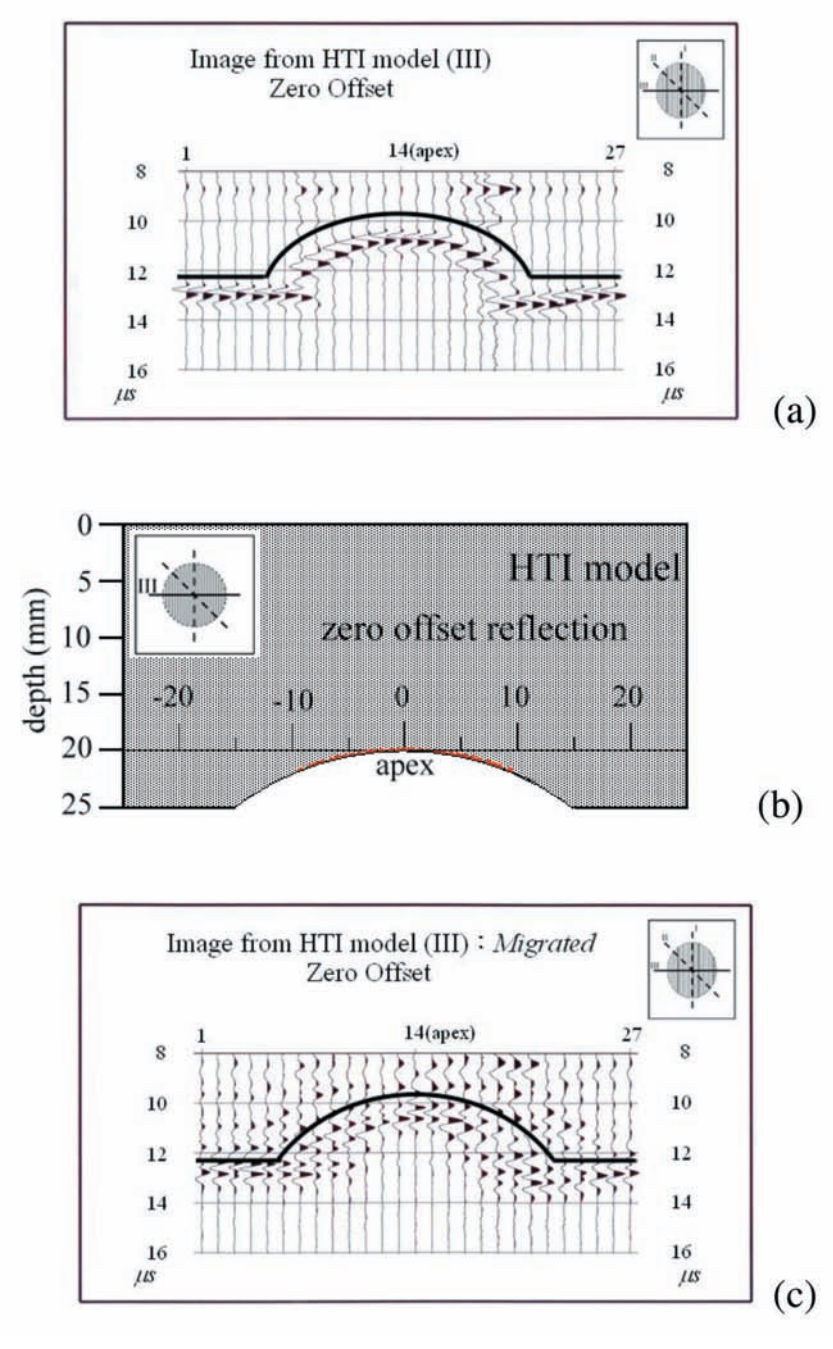

Fig. 6. (a) Zero-offset reflections acquired from the HTI model in the direction of symmetry axis, i.e., layering normal (III). The icon shown in the upper right corner indicates the orientation of the survey line (solid) with respect to the layering of the HTI model. (b) Theoretical reflection points (dots line above the apex) computed by Fermat's principle. (c) Output of the anisotropic 2D Kirchhoff migration.

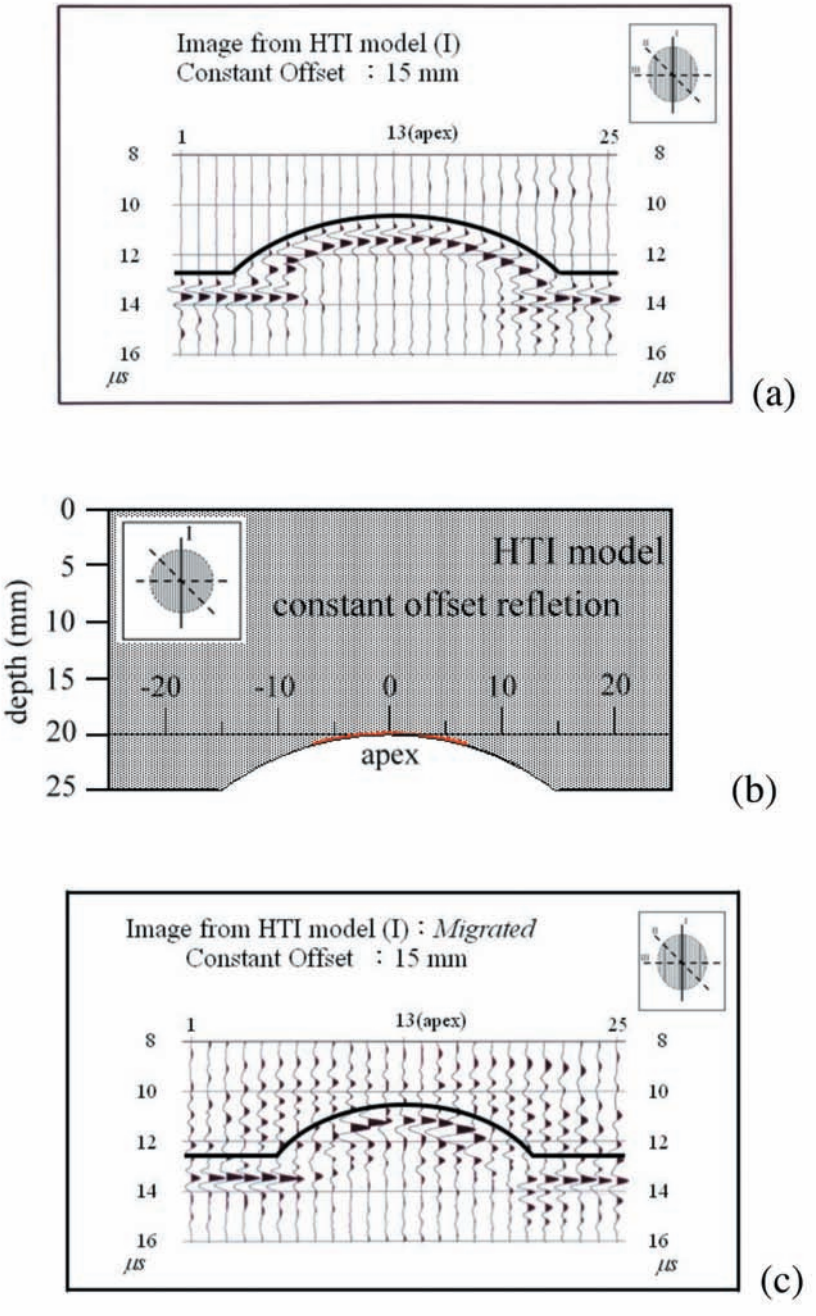

Fig. 7. (a) Constant-offset reflections acquired from the HTI model along layering direction (I). The icon shown in the upper right corner indicates the orientation of the survey line (solid) with respect to the layering of the HTI model. The apex and base reflections were observed at 10.6 μs and 12.8 μs, respectively. (b) Theoretical reflection points (dots line above the apex) computed by Fermat's principle. (c) Output of the anisotropic 2D Kirchhoff migration.

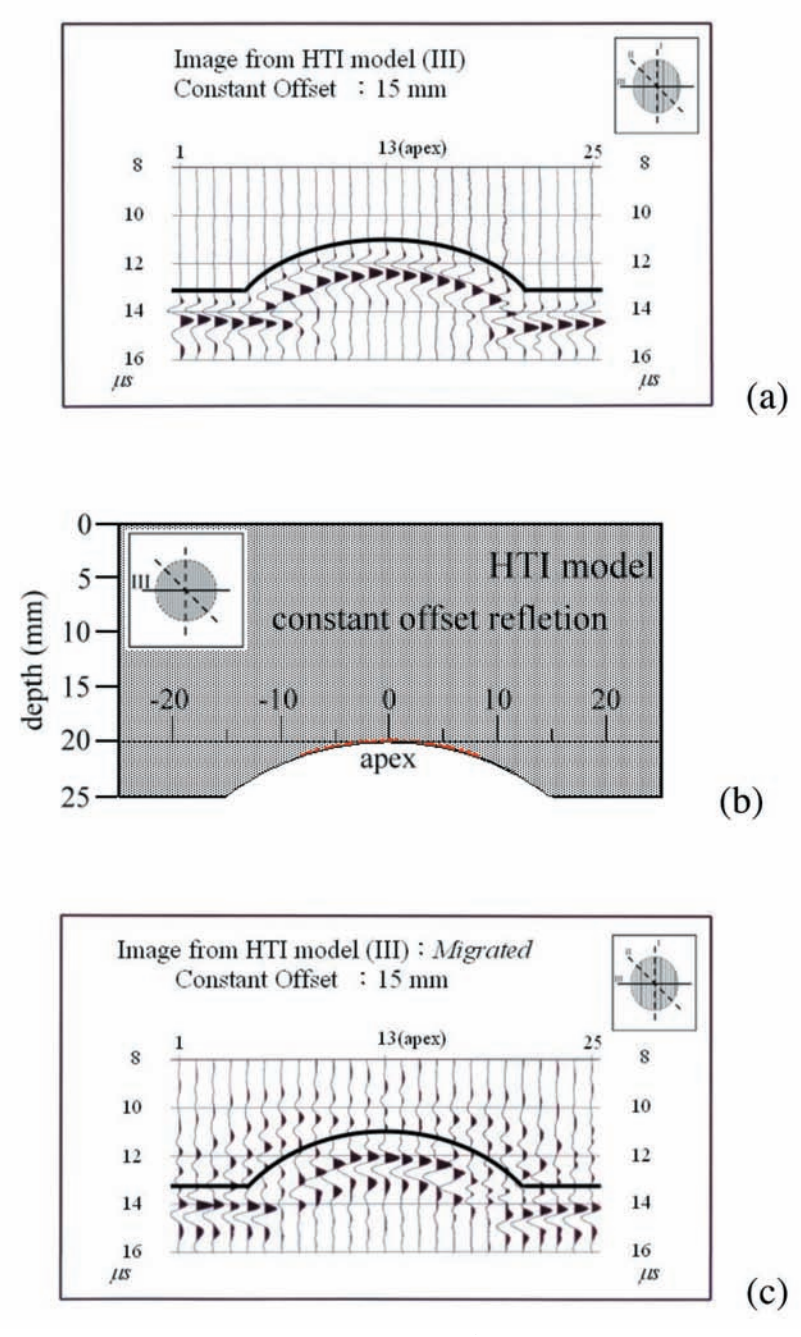

Fig. 8. (a) Constant-offset reflections acquired from the HTI model in the direction of symmetry axis, i.e., layering normal (III). The icon shown in the upper right corner indicates the orientation of the survey line (solid) with respect to the layering of the HTI model. The apex and base reflections were observed at 11.2 μs and 13.2 μs, respectively. (b) Theoretical reflection points (dots line above the apex) computed by Fermat's principle. (c) Output of the anisotropic 2D Kirchhoff migration.

the cause for the observations, theoretical zero-offset reflections were computed by Fermat's principle and shown in Fig. 3(b). The dots line above the apex on the pictorial dome indicate the distribution of theoretical reflection points. Theoretical reflections show that the radius of the imaged dome is approximately 7 mm in zero-offset profiles. For image restoration, laboratory data were processed by anisotropic 2D Kirchhoff migration (Sullivan and Cohen, 1987; Claerbout, 1997). Fig. 3(c) shows the migration output, assuming the raypath of both incidence and reflection falls on the same vertical plane. Due to imperfect reflections collected from the flank of the spherical dome, only the upper portion of the dome structure is resolved in the migrated profile. The dashed curve in Fig. 3(c) was delineated from the migrated dome image. Although the appearance of the actual spherical dome cannot be successfully reconstructed, the error percentage of overestimation in the base of the image is significantly reduced from 58% to 17%. Comparison of theoretical reflections [Fig. 3(b)] in pictorial with migrated profile [Fig. 3(c)] confirms the scheme of migration used.

Following the same layout arrangement [Fig. 2(d)], Fig. 4(a) shows one of the constant-offset reflections collected for the VTI model. Due to polar velocity anisotropy, all three reflection profiles appear as replicas of each other. However, the image of the spherical dome is severely stretched. The diameter of the base of the imaged dome is overestimated by 83%. Theoretical constant-offset reflections computed by Fermat's Principle are shown in Fig. 4(b). Based on theoretical reflections, the radius of the imaged dome is reduced to 4 mm in constant-offset profiles. Fig. 4(c) shows the output of the reconstructed images after laboratory data were processed by the same migration scheme. From the migrated profiles [Fig. 4(c)], it can be observed that the curvature radius of the reconstructed dome structure is significantly reduced. The base diameter of the spherical dome is reconstructed as 37.5 mm, i.e., the overestimation is reduced from 83% to 25% after migration processing.

From theoretical reflections [Figs. 3(b) and 4(b)], it can be observed that the distribution of the dots line above the apex is limited to radii of 4 to 6 mm, centred at the apex of the dome structure in the VTI model. Lateral shift or sideslip occurs because the component of a propagating wave travels faster in a direction perpendicular to the symmetry axis of a TIM. Polar velocity anisotropy induces symmetrically lateral extension in seismic images for both zero-offset and constant-offset reflections in the VTI model. Although lateral extension of the seismic image was significantly improved by the migration technique, true size and shape of the dome structure still cannot be accurately determined.

Reflections in the HTI model

In an HTI model, the azimuthal velocity of a propagating wave varies on the horizontal symmetry axis plane, i.e., orthogonal plane. In order to explore the effects of azimuthal velocity anisotropy on seismic images, zero-offset and constant-offset reflection experiments were carried out on the orthogonal plane in three directions: layering (Line I), layering diagonal (Line II) and layering transverse (Line III) [Fig. 2(d)]. Figs. 5(a) and 6(a) show zero-offset reflection profiles acquired in the layering direction and layering transverse in the HTI model, respectively. The icon shown in the upper right in Figs. 5(a) and 6(a) indicates the layout direction. The diameter of the dome structure was laterally extended by 33% along Line I [Figs. 5(a)] and 17% along Line III [Figs. 6(a)]. The subtle differences in the reflections observed from different directions indicate that the spherical dome structure is not successfully imaged. Due to the intrinsic azimuthal velocity anisotropy of HTI, the created spherical dome is inaccurately imaged as an ellipsoidal dome. The imaged dome has the major and minor axes oriented along layering direction (Line I) and layering normal (Line III), respectively. Figs. 5(b) and 6(b) show theoretical constant-offset reflections in the directions of layering and the symmetry axis. Figs. 5(b) and 6(b) show that the graphical representation of the boundary of the dome structure imaged in HTI became broader. The radii of imaged dome ranged from 7 to 9 mm in zero-offset profiles. Figs. 5(c) and 6(c) show the outputs of migration after laboratory data, i.e., Figs. 5(a) and 6(a), were processed by anisotropy migration. Migrated profiles reveal that the effect of lateral extension of the reflection image is significantly reduced in the layering direction but less in the layering normal. However, a spherical dome was restored in the migrated profiles. Comparison of migrated profiles [Figs. 5(c) and 6(c)] and theoretical reflection [Figs. 5(b) and 6(b)] in pictorial profiles shows good agreement.

Following the same layout arrangement, Figs. 7(a) and 8(a) show the constant-offset reflections acquired from the HTI model. Once again, the spherical dome was imaged as an ellipsoidal dome. The major axis of the imaged dome is measured as 45 mm in the layering direction (Line I), and the minor axis is measured as 40 mm in the direction of layering normal (Line III). The overestimations turn out to be 50% for Line I and 33% for Line III. In other words, directional dependence of the sideslip induced by lateral extension of reflections becomes even more significant in constant-offset reflections when compared to those observed in zero-offset reflections (Figs. 5(a) and 6(a)]. Figs. 7(b) and 8(b) show imaged theoretical reflections and Figs. 7(c) and 8(c) shows the migration outputs. Based on Figs. 7(b) and 8(b), it can be estimated that the radial coverage of the image ranged from 6 mm to 8 mm for constant-offset reflections. The mismatches in the reflection profiles shown in Figs. 7(a) and 8(a) reveal that the effects of azimuthal velocity anisotropy not only lead to lateral movement but also to vertical shifting of constant-offset reflections. In

addition, the inability to trace a circular base from migrated profiles indicates that the spherical nature of the dome was not correctly imaged.

Because a P-wave travels faster along the layering direction than along the symmetry axis direction, the reflections shown in Fig. 7(a) were detected earlier than those shown in Fig. 8(a). Motivated by traveltime differences, we evaluate the feasibility of estimating Thomsen's P-wave anisotropy parameter (ε) from our laboratory observations. Since the propagating P-wave travels with a unique velocity along the layering direction in a TIM, all mathematical manipulations of P-wave behaviour in the layering planes can be treated as an isotropic problem. Hence, the P-wave move-out velocity ($V_{P//}$) in the layering plane can be directly computed by the Pythagorean Theorem to be 4030 m/s. Following the simplified non-hyperbolic move-out formula proposed by Chang and Chang (2003), the P-wave velocity ($V_{P\perp}$) along the fracture normal was computed to be 2891 m/s. Because the phase and group velocities of a propagating P-wave are identical to each other when a measurement is performed along the principal symmetry axes of the TIM, the anisotropy parameter (ε) can be directly estimated from $V_{P//}$ and $V_{P\perp}$. The anisotropy parameter (ε) deduced from $V_{P//}$ and $V_{P\perp}$ is 0.47 and that of the modelling material was measured as 0.48. The feasibility in deducing the P-wave anisotropy parameter (ε) in a HTI medium using traveltime differences of reflections collected in the directions of layering and symmetry axis is thus demonstrated.

Time slice images

To characterize the distortion of images caused by lateral extension in TIM, time slices were delineated based on laboratory observations [Figs. 3(a)-8(a)] versus theoretical arrival times [Figs. 3(b)-8(b)] and laboratory observations [Figs. 3(a)-8(a)] versus migration outputs [Figs. 3(c)-8(c)] at specific arrival times. Time slices obtained from reflection data and theoretical arrivals are displayed adjacently in Fig. 9 to demonstrate the deviation between acquired and theoretical images. Dotted and solid contours shown in Fig. 9 were individually chosen and sketched from the observed (•) and theoretical (★) data. Both VTI and HTI models indicate that the amount of lateral shifting is much more significant for zero-offset reflections [Figs. 9(a) and 9(c)] than for constant-offset reflections [Figs. 9(b) and 9(d)].

Fig. 10 shows time slices obtained from laboratory observations (•) and migration outputs (*). Dotted contours were delineated from laboratory observations and dashed contours were traced from migration outputs. Figs. 10(a) and 10(b) reveal that the images from the VTI model were migrated as spherical domes with small curvature radii. Nonetheless, the true geometry of the spherical dome still could not be satisfactorily resolved. On the other hand,

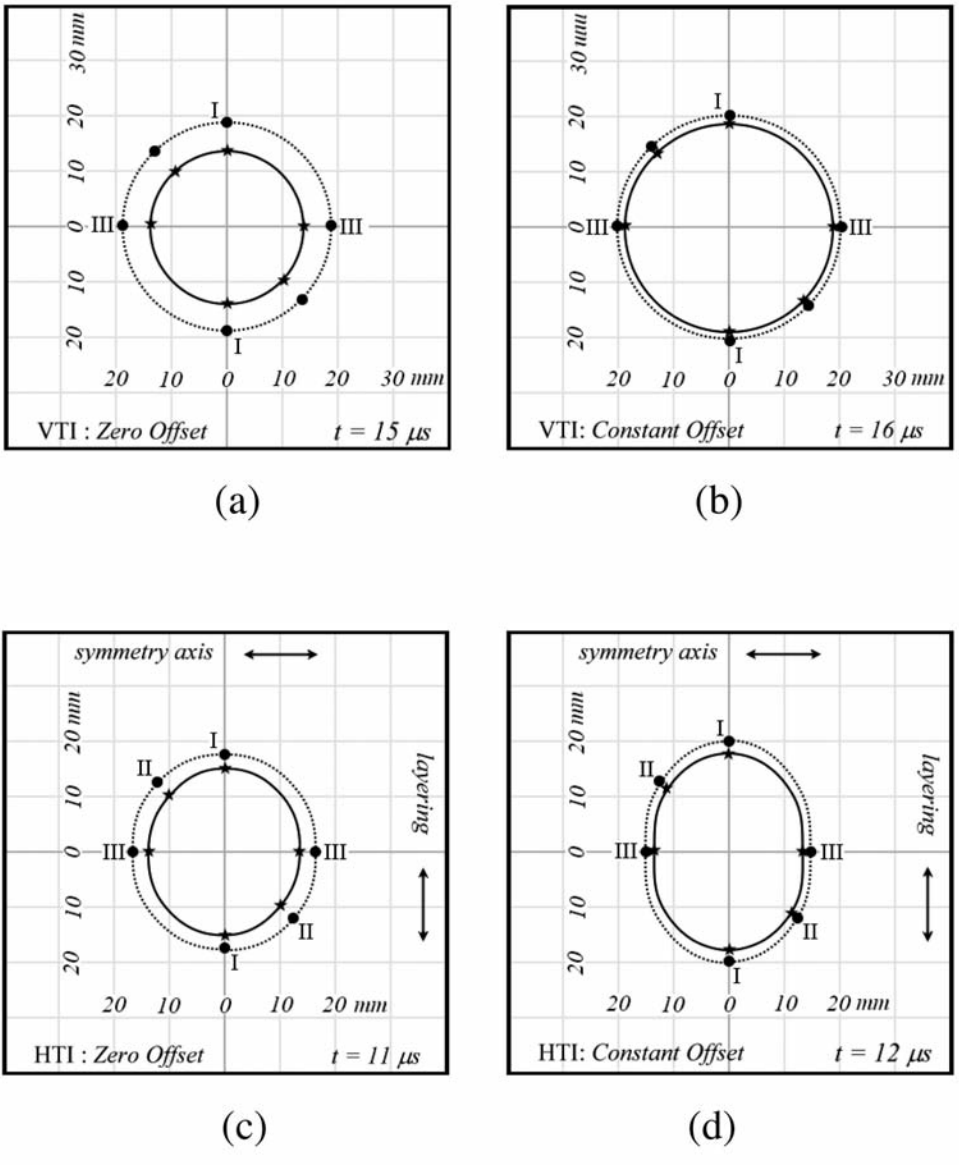

Fig. 9. Time slices delineated from theoretical arrival times (★) computed from the Fermat's principle and laboratory observations (•). (a) zero-offset reflections of VTI at 15 μs, and (b) constant-offset reflections of VTI at 16 μs, (c) zero-offset reflections of HTI at 11 μs, and (d) constant-offset reflection of HTI at 12 μs.

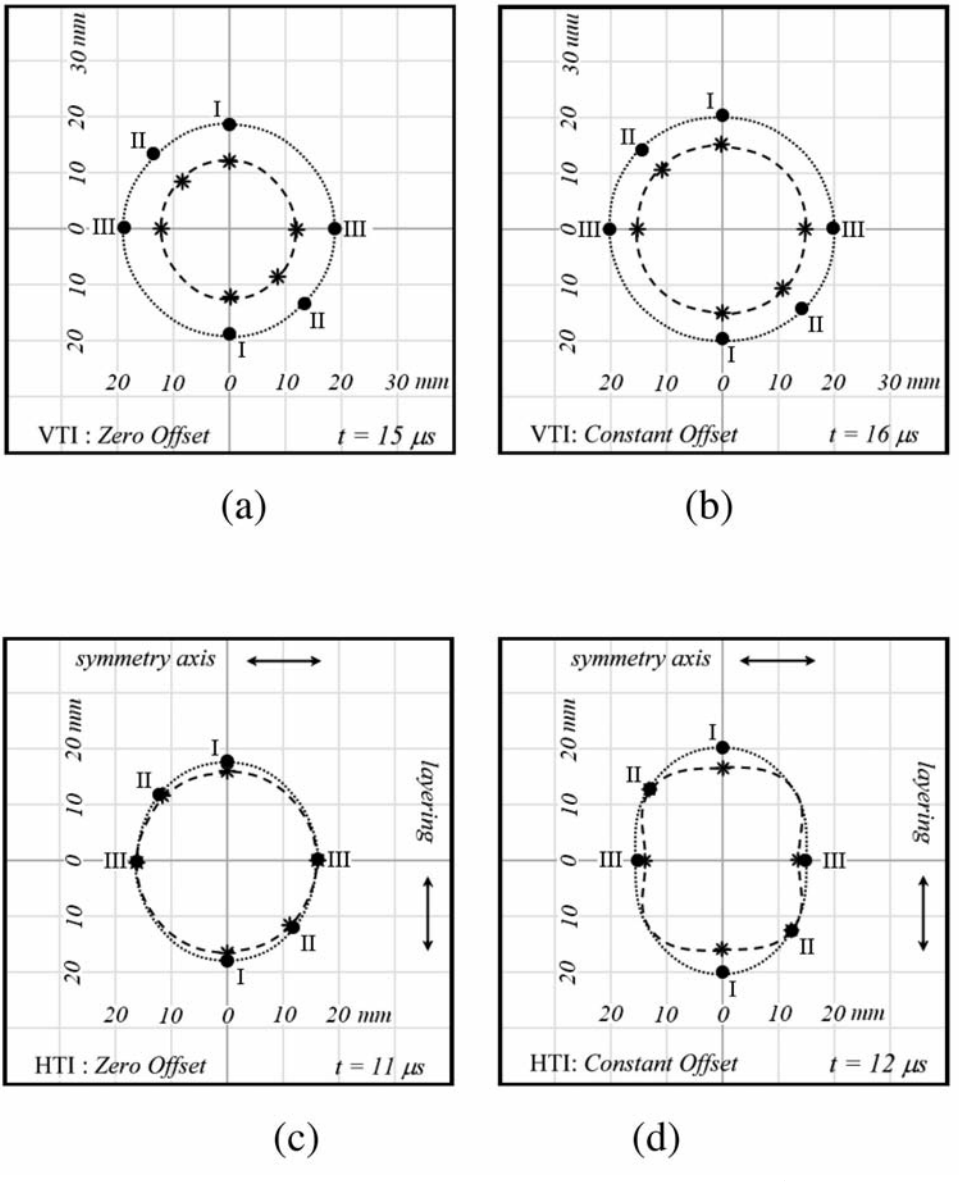

Fig. 10. Time slices delineated from laboratory observations (•) and the outputs of 2D Kirchhoff anisotropy migration (*). (a) zero-offset reflection of VTI at 15 μs, (b) constant-offset reflection of VTI at 16 μs, (c) zero-offset reflection of HTI at 11 μs, and (d) constant-offset reflection of HTI at 12 μs.

the dashed contour shown in Fig. 10(c) indicates that the ellipsoidal dome, imaged from the HTI model in the zero-offset reflection profiles, was migrated to a spherical dome. However, the dashed contour shown in Fig. 10(d) implies that the spherical dome image was not fully resolved from constant-offset reflection profiles in the HTI model. Instead of a circular contour, a flower contour was delineated based on the migration outputs in the horizontal display.

The effect of lateral stretch on seismic images, in both layering and symmetry axis direction, is significantly reduced by migration processing [Fig. 10(d)]. However, constant-offset reflections acquired at 45 degrees to the symmetry axis did not respond well to anisotropic migration. The unsatisfactory image restoration diagonal to the axis of symmetry could be due to the azimuthal dependence of energy propagation in the source-receiver azimuth and the offset on the surface (Cheng et al., 2012). Fig. 10 thus demonstrates the performance of the anisotropic 2D Kirchhoff migration.

DISCUSSIONS

In the presence of anisotropy, the wavefronts spreading from a point source are no longer circles, with the propagating energy traveling more rapidly in the isotropic plane of a TIM. Thus, the velocity of a seismic wave is faster in the layering direction than in the symmetry axis, making the curvature radius of the image of the spherical dome larger than the actual one (Martin et al., 1992). Based on visual inspection, the polar velocity variation in the VTI model caused the diameter of the spherical dome image to be extended by approximately 58% in zero-offset reflections and 83% in constant-offset reflections. Subject to azimuthal velocity anisotropy, the spherical dome was imaged as an ellipsoidal dome in the HTI model. The imaged ellipsoidal dome has the major axis parallel to the direction of layering, i.e., the fastest velocity direction, and the minor axis oriented in the direction of the symmetry axis, i.e., the slowest velocity direction. The phenomenon of a laterally stretched image in both zero-offset and constant-offset reflection profiles was demonstrated in our laboratory observations in both the VTI and HTI models.

The reason for the distorted images obtained in the scaled TI model can be inferred from time slices (Fig. 9). Based on the theoretical computation, the zero-offset reflection images in VTI [Fig. 9(a)] exhibit more lateral extension than those observed in HTI [Fig. 9(c)]. This is due to the propagating P-wave having a more concave curvature wavefront in HTI; correspondingly, less lateral extension in the reflections was observed in our laboratory data (Okoye et al., 1995). Although the images in the constant-offset reflections [Figs. 9(b) and 9(d)] cannot be completely predicted by theoretical computation, the similarity in the contours confirms experimental results. In addition, the elliptical contour

in the time slice of Fig. 9(d) clearly indicates the distortion of the image of the spherical dome in the HTI model. The cause for the distorted image obtained in constant-offset reflections can be attributed to mispositioning induced by azimuthal velocity anisotropy and the directional dependence of downward movement in the reflections.

For image restoration, group velocity models based on the premeasured elastic constants were incorporated into the scheme of anisotropic 2D Kirchhoff migration. Although ambient migration noises, i.e., frowns, caused by the non-interference of the semicircles remained in the migrated profile, the effect of lateral stretching in the images was efficiently suppressed. The decrease in the curvature radius of the restored dome image in the migrated profile affirms the performance of the anisotropic migration. Due to the lack of incident energy on the sides of the spherical dome, a loss of focus on the flanks was observed in the migrated section. The similarity between theoretical computation [Figs. 3(b) to 8(b)] and migration outputs [Figs. 3(c) to 8(c)] further demonstrates the effectiveness of this method. Because the ratio of the depth of the imaged target to the width of the active transducer is approximately 7, the propagating velocity measured in the reflection experiments may not reflect a pure mode of phase or group velocity (Dellinger and Vernik, 1994), and imperfectly destructive interference may have occurred as a result of migration noise (Yilmaz, 1987). On the other hand, lateral velocity variation could be another potential factor leading to residual semicircular "smiles" in the resulting migrated profile.

In addition to the distorted image, which is caused by reflection misposition, "mis-tie" in arrivals originating from the CDP was observed in the HTI model. In the constant-offset profiles, the apex and base reflections were detected earlier, at 10.6 μs and 12.8 μs, in the layering direction, i.e., the fastest velocity orientation [Fig. 7(a)], and later, at 11.2 μs and 13.2 μs, in the direction of layering normal, i.e., the slowest velocity orientation [Fig. 8(a)]. The arrival time difference thus provides a feasible way to estimate the P-wave anisotropy parameter (ε). By means of the simple symmetry properties of the TIM and Pythagoras' theorem, the Thomsen's P-wave anisotropy parameter (ε) was computed to be 0.47, which is nearly equivalent to the modelling material (0.48).

CONCLUSIONS

The complexities of wave behaviour in an anisotropic medium have become a popular topic in reflection seismology and have been widely studied. To investigate the problems of distorted images induced by intrinsic anisotropy, both zero-offset and constant-offset reflections were acquired from VTI and HTI models to image a spherical dome, which was carved into the base of the models. Induced by a lateral shift in reflections, results of our laboratory

observations clearly demonstrate the phenomenon of reflection mispositioning in TIM. Subjected to polar variation, the spherical dome was imaged with a larger radius of curvature in the VTI model. Furthermore, the spherical dome was imaged as an ellipsoidal dome in HTI due to azimuthal velocity anisotropy. Laboratory data show that the effects of lateral stretch, which drift into the seismic image and lead to an overestimation in the subsurface reservoir, are inevitable in a TI area. Hence, unless the problems that cause the distorted image can be properly dealt with, a true subsurface structure cannot be accurately imaged from seismic reflections. Under azimuthal velocity variation, a spherical dome scanned along directions parallel to, at 45 degrees to and perpendicular to the fastest orientation of the HTI model was imaged at different arrival times in the constant-offset profiles. Making use of the arrival time difference between the apex reflections observed in directions parallel to and perpendicular to the fastest velocity orientation of the TI material, we show that the P-wave anisotropy parameter (ε) can be reliably estimated. Our results support the methodology and the feasibility of estimating Thomsen's anisotropy parameters using traveltime difference observed from the CDP in an area of systematically and vertically aligned fractures.

ACKNOWLEDGEMENTS

We wish to express our appreciation to the anonymous reviewer for providing the very constructive suggestions and comments in revising this paper. Our appreciations also go to Dr. Gerald A. Rau for spending his valuable time in editing this paper. The research leading to this paper was financially supported by the National Science Council under grant No. NSC 100-2116-M-415-001-.

REFERENCES

Chang, C.H. and Chang, Y.F., 2003. A simplified nonhyperbolic moveout formula for a transversely isotropic medium. TAO, 14: 99-112.

Cheng, J.B., Wang, T.F., Wang, C.L. and Geng, J.H., 2012. Azimuth-preserved local angle-domain prestack time migration in isotropic, vertical transversely isotropic and azimuthally anisotropic media. Geophysics, 77: S51-S64.

Claerbout, J., 1997. Introduction to Kirchhoff Migration Programs. Stanford Exploration Project, Report 73: 385-391.

Dellinger, J. and Vernik, L., 1994. Do traveltimes in pulse-transmission experiments yield anisotropic group or phase velocity? Geophysics, 59: 1774-1779.

French, W.S., 1974. 2-D and 3-D migration of model-experiment reflection profiles. Geophysics, 39: 265-277.

Grechka, V., Theophanis, S. and Tsvankin, I., 1999. Joint inversion of P- and PS-waves in orthorhombic media: Theory and a physical modeling study. Geophysics, 64: 146-161.

Holt, R., 2006. Constraining anisotropy - Lessons from 2D modeling. Abstr., CSEG-CWLS Convent.: 296-299.

Helbig. K., and Thomsen. L., 2005. 75-plus years of anisotropy in exploration and reservoir seismics: A historical review of concepts and methods. Geophysics, 70: 9ND-23ND.

Isaac, J.H. and Lawton, D.C., 1999. Image mispositioning due to dipping TI media: A physical seismic modeling study. Geophysics, 64: 1230-1238.

Mah, M. and Schmitt, D.R., 2003. Determination of the complete elastic stiffnesses from ultrasonic phase velocity measurements. J. Geophys. Res., 108: ECV 6-1−6-11. doi: 10.1029/2001jb001586.

Martin, D., Ehinger, A. and Rasolofosaon, P., 1992. Some aspects of seismic modeling and imaging in anisotropic media using laser ultrasonics. Expanded Abstr., 62nd Ann. Internat. SEG Mtg., New Orleans: 1373-1376. doi: 10.1190/1.1821998

Okoye, P.N., Uren, N.F., McDonald, J.A. and Ebrom, D.A., 1995. The dependence of lateral resolution on the orientation of symmetry axis and elastic parameter in transversely isotropic media. Expanded Abstr., 65th Ann. Internat. SEG Mtg., Houston: 567-571. doi: 10.1190/1.1887425.

Okoye, P.N. and Uren, N.F., 2000. Fresnel zones and spatial resolution for P- and SH-waves in transversely isotropic media. Geophysics, 65: 1168-1178. doi: 10.1190/1.1444810.

Sullivan, M.F. and Cohen, J.K., 1987. Prestack Kirchhoff inversion of common-offset data. Geophysics, 52: 745-754. doi: 10.1190/1.1442341

Thomsen, L., 2002. Understanding Seismic Anisotropy in Exploration and Exploitation. SEG-EAGE Distinguished Instructor Series, 5. SEG, Tulsa, OK.

Vestrum, R.W. and Fowler, P.J., 2005. Quantifying imaging and position problems beneath TTI media. Extended Abstr., 67th EAGE Conf., Madrid: E026.

Vestrum, R. and Lawton, D., 2010. Reflection point sideslip and smear in imaging below dipping anisotropic media. Geophys. Prosp., 58: 541-548.

Waluyo, W., Uren, N.F. and McDonald, J.A., 1995. Poisson's ratio in transversely isotropic media and its effects on amplitude response: An investigation through physical modelling experiments. Expanded Abstr., 65th Ann. Internat. SEG Mtg., Houston: 585-588.

Wild, P., 2011. Practical applications of seismic anisotropy. First Break, 29: 117-124.

Yilmaz, O., 1987. Migration and ambient noise. In: Doherty, S.M. (Ed.), Seismic Data Processing. SEG, Tulsa, OK: 324-328.